Improving the efficiency of solution processable organic photovoltaic devices by a star-shaped molecular geometry

Chang He,[a] Qingguo He,*[b] Yuanping Yi,[a] Guanglong Wu,[a] Fenglian Bai,[a] Zhigang Shuai[a] and Yongfang Li*[a]

Received 1st May 2008, Accepted 25th June 2008
First published as an Advance Article on the web 21st July 2008
DOI: 10.1039/b807456a

A new solution processable star-shaped organic molecule S(TPA-BT) has been synthesized for application in organic solar cells (OSCs). The properties and structures of S(TPA-BT) and a related linear molecule L(TPA-BT) were studied, including UV-visible spectroscopy, hole charge mobility, and theoretical calculated geometry and electronic properties. S(TPA-BT) film shows a broader and stronger absorption band in the range of 440–670 nm, lower band gap of 1.86 eV, higher hole mobility of 4.71×10^{-5} cm^2 V^{-1} s^{-1} and better film-forming properties compared with those of L(TPA-BT) film. ITO/PEDOT:PSS/S(TPA-BT) or L(TPA-BT):PCBM/Ba/Al bulk-heterojunction OSCs were fabricated with S(TPA-BT) or L(TPA-BT) as donor material. The power conversion efficiency (PCE) of an OSC based on a blend of S(TPA-BT) and PCBM (1 : 3, w/w) reached 1.33% under A.M. 1.5 illumination, 100 mW cm^{-2}, with a short-circuit current density (J_{SC}) of 4.18 mA cm^{-2}, an open circuit voltage of 0.81 V, and a fill factor of 39%. The PCE of 1.33% and J_{sc} of 4.18 mA cm^{-2} are among the highest values reported so far for solution processable OSCs.

Introduction

Solution processable small molecules have attracted more and more attention as active materials in organic solar cells (OSCs)[1,2] and organic light-emitting diodes (OLEDs)[3] due to their high purity and good reproducible optoelectronic properties. Recently considerable research efforts have led to major progress in the synthesis of new solution processable organic photovoltaic molecules.[4–12] The maximum power conversion efficiency (PCE) of a solution processable bulk-heterojunction device based on an anthradithiophene derivative as the donor blended with a C_{60} derivative [(6,6)-phenyl C_{61} butyric acid methyl ester (PCBM)] as acceptor material reached 1%.[12] However, the PCEs of OSCs based on solution processable small molecules are much lower than those of polymer based solar cells which have shown PCEs higher than 5%.[13] The PCEs of OSCs based on solution processable small molecules are mainly restricted by limited light absorption of the active layer of the device, lower hole mobility of the molecules, and are also affected by the quality of the spin-coated film of the active layer. These crucial properties are closely related to the chemical structure of the molecules used as the active layer of the device. Thus, it is vital to understand the relationship between the structure design and properties of solution processable organic compounds which play key roles for obtaining higher PCE OSCs.

Here we report a new solution processable star-shaped organic molecule S(TPA-BT) (as shown in Scheme 1) with three D–π–A–π–D structured branches based on triphenylamine (TPA) as core and donor units (D), benzothiadiazole (BT) as acceptor units (A), and the ethylene double bonds as π-connections between them, for application in OSCs. The design of the molecular structure was from the following considerations: (1) the TPA-based star-shaped molecules possess three-dimensional spatial structure with good solution processability and have been used in electroluminescence[14] and photovoltaics;[15] (2) the D–π–A structure is in the molecule to reduce the bandgap of the material and make its absorption spectrum match with the solar spectrum; (3) the TPA end groups are for further improving its solubility and enhancing its hole mobility because TPA is a typical hole transporting group. S(TPA-BT) film shows a broader and stronger absorption band in the range of 440–670 nm, a lower band gap of 1.86 eV, a higher hole mobility of 4.71×10^{-5} cm^2 V^{-1} s^{-1} and better film-forming properties than those of the corresponding linear L(TPA-BT). The PCE of an OSC based on a blend of S(TPA-BT) and PCBM (1 : 3, w/w) reached 1.33% under A.M. 1.5 illumination, 100 mW cm^{-2}, which is among the highest values reported so far for solution processable OSCs.

Experimental

All chemicals were purchased from Aldrich or Acros Chemical Co. and were used without further purification, except that DMF was freshly distilled prior to use. Compounds **1** and **3** were synthesized according to literature procedure,[16] compound **2** was synthesized according to a prior report.[17] The linear molecule L(TPA-BT) was also synthesized according to the literature.[18] The synthesis routes to L(TPA-BT) and S(TPA-BT) are shown in Scheme 1.

[a]*Beijing National Laboratory for Molecular Sciences, Key Laboratory of Organic Solids, Institute of Chemistry, Chinese Academy of Sciences (CAS), Beijing, 100080, China. E-mail: liyf@iccas.ac.cn; Fax: +86-10-62559373; Tel: +86-10-62536989*
[b]*Institute of Microsystems and Information Technology, CAS, Shanghai, 200050, China. E-mail: hqg@mail.sim.ac.cn; Fax: +86-21-62511070; Tel: +86-21-62511070*

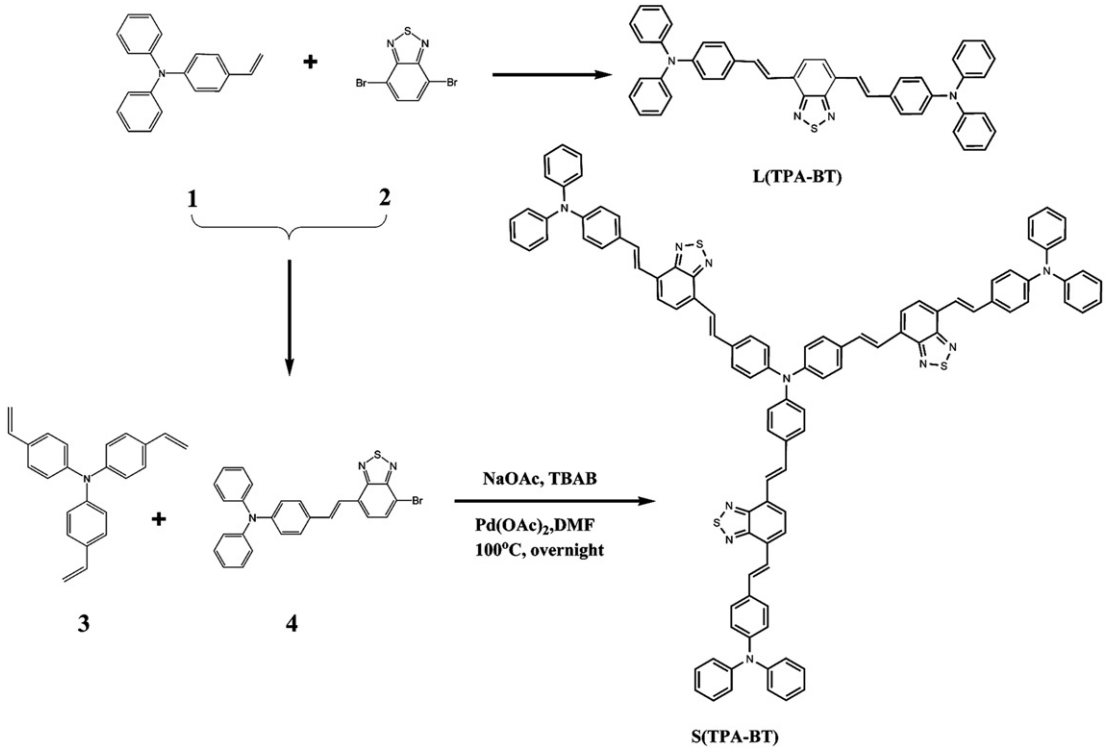

Scheme 1 Synthesis routes to L(TPA-BT) and S(TPA-BT).

Synthesis of compound 4

A mixture of *N*-phenyl-*N*-(4-vinylphenyl)benzeneamine compound **1** 1.57 g (5.8 mmol), 4,7-dibromobenzo[*c*][1,2,5]thiadiazole compound **2** 1.705g, $Pd(OAc)_2$ 26 mg (2% molar amount), NaOAc 4.76 g (58 mmol) and *n*-Bu_4NBr 0.30 g (0.928 mmol) was dissolved in 60 mL freshly distilled and degassed DMF. The solution was kept at 100 °C for 24 h. Then 100 mL distilled water was added. The precipitate was filtered off, washed with water, and dissolved in methylene chloride, then dried over $MgSO_4$. After the solvent was evaporated off under reduced pressure, it was subjected to column separation (SiO_2, petroleum ether–methane chloride 3 : 1). 671 mg of compound **4** were obtained with a yield of 24%. ^{1}H NMR (δ/ppm): 7.04 (m, $J = 8.7$, 8.0 Hz, 4 H), 7.12 (d, $J = 8.0$ Hz, 4 H), 7.28 (d, $J = 7.7$, 4 H), 7.44 (d, $J = 16.3$, 1 H), 7.49–7.53 (m, 3 H), 7.81 (d, $J = 7.5$ Hz, 1 H), 7.89 (d, $J = 16.3$ Hz, 1 H). ^{13}C NMR (δ/ppm): 111.72, 121.69, 122.99 (×2), 123.36 (×2), 124.80 (×4), 126.11, 127.90 (×2), 129.34 (×4), 130.63, 130.90, 132.13, 133.77, 147.33 (×2), 148.17, 152.96, 153.83. MALDI-TOF MS: calcd for $C_{26}H_{18}BrN_3S$ 483.04; found 483.4.

Synthesis of S(TPA-BT)

To a two-necked glass vessel connected with condenser and balloon were added *N*-(4-((*E*)-2-(4-bromobenzo[*c*][1,2,5]thiadiazol-7-yl)vinyl)phenyl)-*N*-phenylbenzeneamine (compound **4**) (0.36 g, 0.74 mmol), tris(4-vinylphenyl)amine (compound **3**) (72.8 mg, 0.225 mmol), $Pd(OAc)_2$ (10 mg, 3.3×10^{-2} mmol), NaOAc (0.277 g, 3.38 mmol) and tetrabutylammonium bromide (43 mg, 1.35×10^{-1} mmol). Degassed and freshly distilled DMF (10 mL) was injected. Then the reaction mixture was heated to 100 °C and kept overnight. Then 20 mL water was poured into the solution to stop the reaction. The violet precipitate was filtered off and washed with water. The violet solid was dissolved in methylene chloride and dried over $MgSO_4$. Further purification was conducted *via* short column separation (SiO_2, CH_2Cl_2). 307.5 mg of a violet solid was obtained in a yield of 88.4%. The structure and purity of S(TPA-BT) were confirmed by ^{1}H and ^{13}C NMR spectroscopy and MALDI-TOF mass spectrometry. ^{1}H NMR (300 MHz, $CDCl_3$, δ/ppm): 7.03–7.10 (m, 12 H), 7.12 (d, $J = 7.78$ Hz, 12 H), 7.17 (d, $J = 8.46$ Hz, 6 H), 7.28 (d, $J = 7.96$ Hz, 12 H), 7.5–7.6 (m, 18 H), 7.66 (s, 6 H), 7.90 (d, $J = 12.4$ Hz, H), 7.96 (d, $J = 12.4$ Hz, H);^{13}C NMR (600 MHz, $CDCl_3$, δ/ppm): 112.69, 123.24, 123.31, 123.40, 124.32, 124.73, 126.30, 126.62, 127.83, 128.09, 128.96, 129.28, 129.46, 131.51, 132.11, 132.46, 132.58, 146.85, 147.54, 148.03, 153.87, 153.90; MALDI-TOF MS: calcd for $C_{102}H_{72}N_{10}S_3$ 1533.93; found 1534.1.

Characterization

^{1}H NMR and ^{13}C NMR spectra were measured on a Bruker DMX-300 or DMX-600 spectrometer. Thermogravimetric analysis (TGA) was conducted on a Perkin-Elmer TGA-10 instrument with a heating rate of 10 °C min^{-1} under a nitrogen atmosphere. Differential scanning calorimetric measurements (DSC) of the molecule was performed under nitrogen at a heating rate of 10 °C min^{-1} with a Perkin-Elmer DSC-10 calorimeter. Absorption and photoluminescence (PL) spectra were taken on a Hitachi U-3010 UV-Vis spectrophotometer and a Hitachi F-4500 spectrophotometer, respectively. MALDI-TOF-MS was measured on a Bruker BIFLEXIII. The cyclic voltammetry was conducted with a Zahner IM6e electrochemical workstation in

0.1 mol L^{-1} Bu_4NPF_6 acetonitrile solution. A glassy carbon electrode coated with the sample film was used as the working electrode; a Pt wire and Ag/Ag^+ (0.01 M $AgNO_3$ in acetonitrile) were used as the counter and reference electrodes respectively. The atomic force microscopy (AFM) measurement of the surface morphology of samples was conducted on a Nanoscope III (DI, USA) in contacting mode with 5 μm scanner.

Fabrication and characterization of organic solar cells

Organic solar cells were fabricated in the configuration of the traditional sandwich structure with an ITO anode and a metal cathode. Patterned ITO glass with a sheet resistance of 30 Ω $\square^{-1}$ was purchased from CSG Holding Co., Ltd (China). The ITO glass was cleaned in an ultrasonic bath of acetone and isopropanol, and then treated by UVO (ultraviolet ozone cleaner, Jelight Company, USA). Then a thin layer (30 nm) of PEDOT:PSS (poly(3,4-ethylenedioxythiophene)-poly(styrene sulfonate)) (Baytron PVP A1 4083 Germany) was spin-coated on the ITO glass and baked at 150 °C for 0.5 h. Subsequently, the photosensitive layer was prepared by spin-coating the blend chlorobenzene solution of S(TPA-BT) or L(TPA-BT) with PCBM (1 : 3 w/w,) on the top of the PEDOT:PSS layer. The thickness of the photosensitive layers was measured using an Ambios Technology XP-2 profilometer. A metal electrode layer of Ba (10 nm)/Al (*ca.* 100 nm) was deposited on the photosensitive layer by vacuum evaporation with a shadow mask under a base pressure of *ca.* 10^{-4} Pa. The active area of the device was 4 mm^2. The current–voltage (*I–V*) measurement of the devices was conducted on a computer-controlled Keithley 236 Source Measure Unit. A xenon lamp coupled with A.M. 1.5 solar spectrum filters was used as light source, and the optical power at the sample was *ca.* 100 mW cm^{-2}. The input photon to converted current efficiency (IPCE) was measured using a Keithley 2000 System DMM coupled with a WDG3 monochromator and 500 W xenon lamp. The light intensity at each wavelength was calibrated with a standard single-crystal Si photovoltaic cell.

Results and discussion

Synthesis and characterization

S(TPA-BT) was synthesized from **3** and **4** with the Heck reaction, and compound **4** was synthesized from **1** and **2** by the Heck reaction, as shown in Scheme 1. For comparison with the structure–property relationship of the conjugated system, a linear molecule L(TPA-BT) was also synthesized. It should be noted that the yield of S(TPA-BT) is high (88.4%), while that of compound **4** is quite low (24%). Actually, under the reaction conditions for the synthesis of compound **4**, the linear derivative L(TPA-BT) was always obtained as the main product, even when changing the catalyst, varying the feed ratio of the starting materials or tuning the reaction temperatures. However for the synthesis of the star-shaped S(TPA-BT) by the 3-fold Heck reaction, only the target compound was obtained since compound **4** and tris(4-vinylphenyl)amine have sufficient reactivity.

Both S(TPA-BT) and L(TPA-BT) are soluble in common organic solvents, such as $CHCl_3$, THF, chlorobenzene and toluene. The glass transition temperature of S(TPA-BT) is

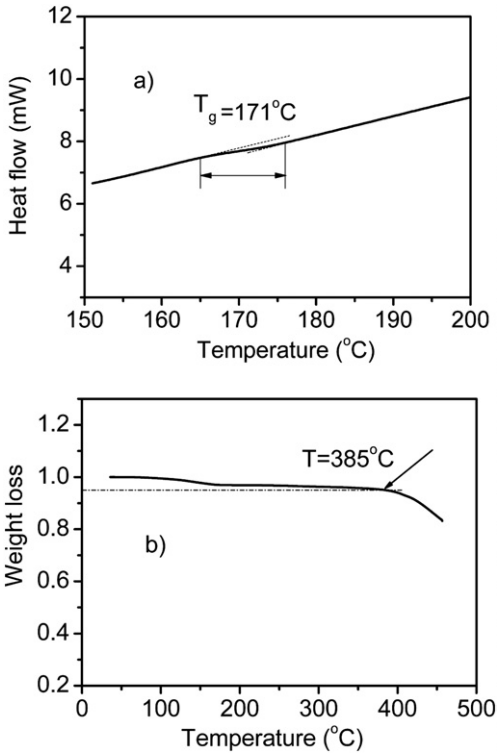

Fig. 1 (a) Differential scanning calorimetry (DSC) measurement of S(TPA-BT), scan rate 10 °C min^{-1}. (b) Thermogravimetric analysis (TGA) of S(TPA-BT).

171 °C, measured by differential scanning calorimetry (DSC) as shown in Fig. 1a. The thermal stability of S(TPA-BT) was investigated by thermogravimetric analysis (TGA), showing a 5% weight loss at 385 °C as shown in Fig. 1b.

The absorption spectrum of S(TPA-BT) solution in chlorobenzene, as shown in Fig. 2a, displays two peaks in the UV-visible region. The UV absorption band with a maximum at 375 nm and a shoulder at 329 nm corresponds to the π–π* absorption of the molecule, and the visible absorption band with a peak at 531 nm could be assigned to the intramolecular charge transfer (ICT) transition between the triphenylamine (TPA) moiety and benzothiadiazole (BT) unit. The L(TPA-BT) solution shows a UV absorption with a maximum at 366 nm and a shoulder at 312 nm, and the ICT band peak at 512 nm. Obviously, the ICT band of S(TPA-BT) is red-shifted by 19 nm in comparison with that of L(TPA-BT). Fig. 2b shows the unit thickness absorbances of S(TPA-BT) and L(TPA-BT) films, which were calculated from their absorbance divided by the film thickness. In comparison with its solution, the ICT band of the S(TPA-BT) film peak at 541 nm red-shifted slightly. Interestingly, the absorption peak of the S(TPA-BT) film is broader and much stronger than that of the L(TPA-BT) film. The ICT absorption band of S(TPA-BT) film covers the wavelength range of 440–670 nm, with a peak absorbance of 1.04×10^{-2} nm^{-1} at 541 nm. The peak absorbance of L(TPA-BT) film is only 0.58×10^{-2} nm^{-1} at 522 nm. The band gap (E_g) of S(TPA-BT) determined from its absorption edge is 1.86 eV which is reduced by 0.14 eV in comparison with the value of 2.0 eV for L(TPA-BT). These results demonstrate that the three-branched star-burst

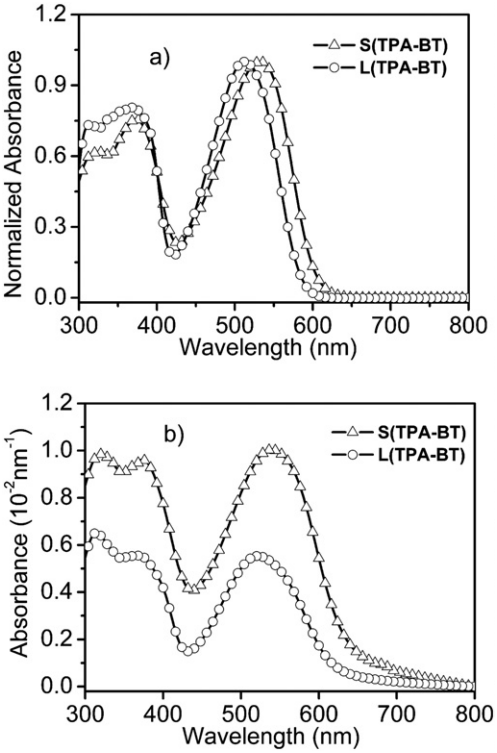

Fig. 2 (a) UV-Vis absorption spectra of S(TPA-BT) and L(TPA-BT) solution in chlorobenzene. (b) Unit thickness absorbance of S(TPA-BT) and L(TPA-BT) films on quartz plates spin-coated from their chlorobenzene solutions.

compound S(TPA-BT) has much stronger light absorption ability than that of the linear molecule L(TPA-BT). These results further indicate that a molecule structure containing an extended π-conjugated system is an efficient method for the design of organic photovoltaic molecules.

In order to determine the HOMO and LUMO energy levels of S(TPA-BT), electrochemical cyclic voltammetry was carried out for a S(TPA-BT) film on a glassy carbon electrode. Fig. 3 shows the cyclic voltammogram of the S(TPA-BT) film. It can be seen that there are a couple of reversible oxidation/re-reduction peaks in the positive potential region with the onset oxidation potential (E_{onset}^{ox}) at 0.59 V *vs.* Ag/Ag^+, and an irreversible reduction peak in the negative potential region with onset reduction potential

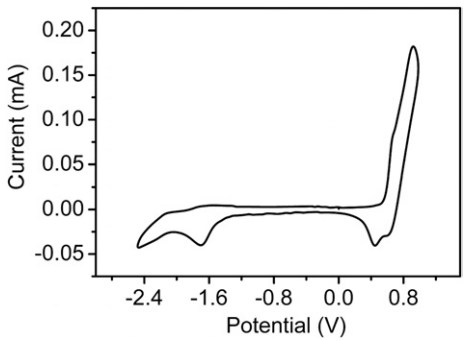

Fig. 3 Cyclic voltammogram of S(TPA-BT) film on glassy carbon electrode in an acetonitrile solution of 0.1 mol/L Bu_4NPF_6 (Bu = butyl) with a scan rate of 20 mV/s.

(E_{onset}^{red}) at −1.44 V *vs.* Ag/Ag^+. The HOMO and LUMO levels were calculated to be −5.3 eV and −3.27 eV respectively, according to the equations: HOMO $= -e(E_{onset}^{ox} + 4.71)$ (eV) and LUMO $= -e(E_{onset}^{red} + 4.71)$ (eV).[19] In comparison with the HOMO level of −6.1 eV and LUMO level of −3.7 eV of PCBM,[20] S(TPA-BT) is suitable for use as a donor material blended with PCBM as acceptor in OSCs.

Charge carrier mobility of photovoltaic materials is another important factor which influences the efficiency of OSCs. The hole mobilities of S(TPA-BT) and L(TPA-BT) films were measured by the space-charge-limited-current method,[21–23] with the device structure of ITO/PEDOT:PSS/S(TPA-BT) or L(TPA-BT)/Au. The results are plotted as $\ln(JL^3/V^2)$ *versus* $(V/L)^{0.5}$, as shown in Fig. 4. The hole mobilities of S(TPA-BT) and L(TPA-BT), calculated from the intercepts of the corresponding lines, are 4.71×10^{-5} cm^2 V^{-1} s^{-1} and 1.46×10^{-6} cm^2 V^{-1} s^{-1} respectively. The hole mobility of S(TPA-BT) is one order higher than that of L(TPA-BT). The 3D spatial geometry of the star-shaped S(TPA-BT) could be beneficial for intra- and intermolecular hole transportation, as it possesses higher hole mobility.

The geometry and electronic properties of S(TPA-BT) and L(TPA-BT) have been investigated by means of theoretical calculation with the Gaussian 03 program package at a hybrid density functional theory (DFT) level.[24] Becke's three-parameter gradient corrected functional (B3LYP) with a 6-31G basis was used for full geometry optimization. Fig. 5 presents the geometry and the highest occupied molecular orbital (HOMO) and the lowest unoccupied molecular orbital (LUMO). For the geometry observed for S(TPA-BT), steric hindrance between the (D–π–A–π–D) arms grafted on the central nitrogen atom generates the propeller shape of molecule. Furthermore, the TPA moieties at the end of each arm increase the multidimensionality of the molecule. This geometry could be beneficial for good solution processability and to forming amorphous films. The HOMO of S(TPA-BT) is mainly distributed on the (D–π–A–π–D) arms with some extending to the central TPA moiety. The LUMO is localized on the benzothiadiazole (BT) electron-withdrawing groups and on the adjacent ethylene unit. The geometry and orbital contribution of L(TPA-BT) are the same as that of the arms of S(TPA-BT). According to the orbital level analysis, the

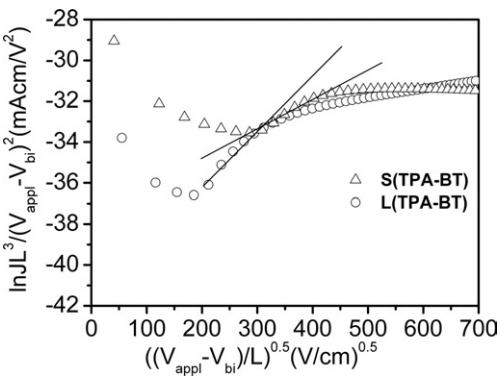

Fig. 4 Current–voltage data from the device ITO/PEDOT:PSS/S(TPA-BT) or L(TPA-BT)/Au, plotted in the format $\ln(JL^3/V^2)$ *versus* $(V/L)^{0.5}$, where J is the current density and L is the thickness of the S(TPA-BT) or L(TPA-BT) layer. The lines are fits to the respective experimental data points.

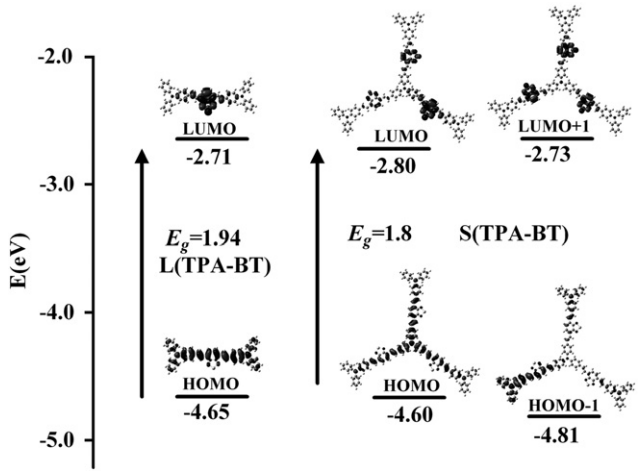

Fig. 5 Calculated HOMO and LUMO levels for compounds L(TPA-BT) and S(TPA-BT).

band gap decreased from 1.94 eV for L(TPA-BT) to 1.8 eV for S(TPA-BT), which agrees well with that obtained from absorption edges.

Photovoltaic properties

Bulk-heterojunction OSCs were fabricated with spin-cast blend films of S(TPA-BT) or L(TPA-BT) and PCBM (1 : 3, w/w) as the active layer and Ba/Al as the cathode. Fig. 6a shows the current–voltage (I–V) curves of the OSCs in the dark and under AM 1.5 illumination, 100 mW cm^{-2}. The open circuit voltage (V_{OC}), short circuit current (I_{SC}), fill factor (FF) and power conversion efficiency (PCE) of the OSC based on S(TPA-BT) reached 0.81 V, 4.18 mA cm^{-2}, 0.39 and 1.33% respectively, under AM 1.5 illumination, 100 mW cm^{-2}, while those of the OSC based on L(TPA-BT) are 0.84 V, 1.25 mA cm^{-2}, 0.34 and 0.35% respectively. Obviously, the photovoltaic behavior of S(TPA-BT) is much better than that of L(TPA-BT). The incident photon-to-converted current efficiency (IPCE) spectra (see Fig. 6b) show similar shapes as those of the absorption spectra of the compounds, indicating that all the visible light absorptions of S(TPA-BT) and L(TPA-BT) contributed to the photovoltaic conversion. The maximum IPCE value of the OSC based on S(TPA-BT) reached 33.2% at 560 nm, which is much higher than that of the device based on L(TPA-BT). The IPCE result is consistent with the higher I_{SC} and PCE values of the S(TPA-BT)-based OSC. The AFM images of the blend films of S(TPA-BT) with PCBM and L(TPA-BT) with PCBM, as shown in Fig. 7, reveal that S(TPA-BT) has better film-forming property compared with L(TPA-BT). The better photovoltaic behavior obtained with S(TPA-BT) as donor should be ascribed to the synergistic effects of its enhanced absorption of incident light, higher hole mobility and high quality uniform spin-cast film.

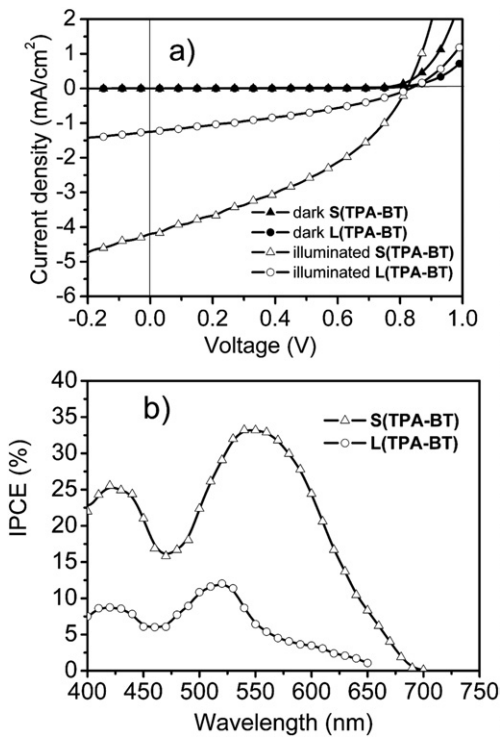

Fig. 6 (a) Current–voltage curves in the and under AM 1.5 illumination, 100 mW cm^{-2}. (b) IPCE spectra of the OSCs based on blend films of S(TPA-BT) or L(TPA-BT) and PCBM (1 : 3, w/w) as the active layer and Ba/Al as the cathode.

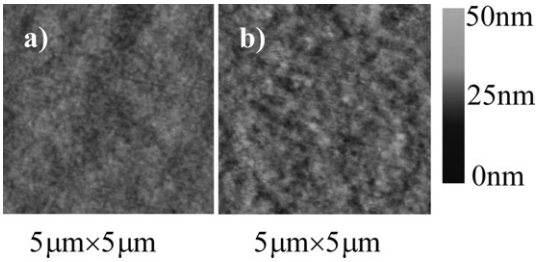

Fig. 7 AFM images of (a) the blend film of S (TPA-BT) : PCBM and (b) the blend film of L(TPA-BT) : PCBM spin-coated from their chlorobenzene solutions.

Conclusions

We designed and synthesized the solution processable star-shaped molecule S(TPA-BT) with D–π–A–π–D structure for solution-processable OSC application based on optimization of the molecular geometry. Compared with linear L(TPA-BT), star-shaped S(TPA-BT) shows broader and stronger absorption in the visible region covering the wavelength range of 440–670 nm, higher hole mobility of 4.71×10^{-5} cm^2 V^{-1} s^{-1}, and appropriate HOMO (−5.3 eV) and LUMO (−3.27 eV) energy levels for use as a donor material with PCBM as acceptor in OSCs. Bulk heterojunction OSCs were fabricated based on blends of L(TPA-BT) or S(TPA-BT) with PCBM (1 : 3, w/w) by spin-coating. The power conversion efficiency of the bulk-heterojunction device based on S(TPA-BT) as donor reached 1.33%, which is 3.8 times greater than that of the device based on L(TPA-BT) under AM 1.5 illumination, 100 mW cm^{-2}. The efficiency of 1.33% is among the highest values reported so far for solution processable OSCs. The results indicate that star-shaped molecules with D–π–A–π–D structure are promising candidates for high efficiency solution processable OSCs.

Acknowledgements

This work was supported by NSFC (Nos. 20574078, 50503024, 50633050 and 20721061, 20773156) and the Ministry of Science and Technology of China (863 project, No. 2006AA03Z220).

References

1 J. Roncali, P. Leriche and A. Cravino, *Adv. Mater.*, 2007, **19**, 2045.
2 M. T. Lloyd, J. E. Anthony and G. G. Malliaras, *Mater. Today*, 2007, **10**, 34.
3 Y. Shirota and H. Kageyama, *Chem. Rev.*, 2007, **107**, 953.
4 S. Roquet, A. Cravino, P. Leriche, O. Alévêque, P. Frere and J. Roncali, *J. Am. Chem. Soc.*, 2006, **128**, 3459.
5 J. Cremer and P. Bäuerle, *J. Mater. Chem.*, 2006, **16**, 874.
6 X. B. Sun, Y. H. Zhou, W. C. Wu, Y. Q. Liu, W. J. Tian, G. Yu, W. F. Qiu, S. Y. Chen and D. B. Zhu, *J. Phys. Chem. B*, 2006, **110**, 7702.
7 C. He, Q. G. He, Y. J. He, Y. F. Li, F. L. Bai, C. H. Yang, Y. Q. Ding, L. X. Wang and J. P. Ye, *Sol. Energy Mater. Sol. Cells*, 2006, **90**, 1815.
8 C. He, Q. G. He, X. D. Yang, G. L. Wu, C. H. Yang, F. L. Bai, Z. G. Shuai, L. X. Wang and Y. F. Li, *J. Phys. Chem. C*, 2007, **111**, 8661.
9 Y. H. Zhou, P. Peng, L. Han and W. J. Tian, *Synth. Met.*, 2007, **157**, 502.
10 M. L. Sun, L. Wang, X. H. Zhu, B. Du, R. S. Liu, W. Yang and Y. Cao, *Sol. Energy Mater. Sol. Cells*, 2007, **91**, 1681.
11 P. Leriche, P. Frère, A. Cravino, O. Alévêque and J. Roncali, *J. Org. Chem.*, 2007, **72**, 8332.
12 M. T. Lloyd, A. C. Mayer, S. Subramanian, D. A. Mourey, D. J. Herman, A. V. Bapat, J. E. Anthony and G. G. Malliaras, *J. Am. Chem. Soc.*, 2007, **129**, 9144.
13 J. Y. Kim, K. Lee, N. E. Coates, D. Moses, T.-Q. Nguyen, M. Dante and A. J. Heeger, *Science*, 2007, **317**, 222.
14 Y. Shirota, *J. Mater. Chem.*, 2005, **15**, 75.
15 A. Cravino, P. Leriche, O. Aleveque, S. Roquet and J. Roncali, *Adv. Mater.*, 2006, **18**, 3033.
16 W. Wenseleers, F. Stellacci, T. Meyer-Friedrichsen, T. Mangel, C. A. Bauer, S. J. K. Pond, S. R. Marder and J. W. Perry, *J. Phys. Chem. B*, 2002, **106**, 6853.
17 K. Pilgram, M. Zupan and R. J. Skiles, *J. Heterocycl. Chem.*, 1970, **7**, 629.
18 S. Kato, T. Matsumoto, M. Shigeiwa, H. Gorohmaru, S. Maeda, T. Ishi-i and S. Mataka, *Chem.–Eur. J.*, 2006, **12**, 2303.
19 Q. J. Sun, H. Q. Wang, C. H. Yang and Y. F. Li, *J. Mater. Chem.*, 2003, **13**, 800.
20 J. C. Hummelen, B. W. Knight, F. Lepeq, F. Wudl, J. Yao and C. L Wilkins,, *J. Org. Chem.*, 1995, **60**, 532.
21 D. Chirvase, Z. Chiguvare, M. Knipper, J. Parisi, V. Dyakonov and J. C. Hummelen, *Phys. Rev. B*, 2004, **70**, 235207.
22 G. G. Malliaras, J. R. Salem, P. J. Brock and C. Scott, *Phys. Rev. B*, 1998, **58**, 13411.
23 H. C. F Martens, H. B. Brom and P. W. M. Blom, *Phys. Rev. B*, 1999, **60**, 8489.
24 M. J. Frisch, G. W. Trucks, H. B. Schlegel, G. E. Scuseria, M. A. Robb, J. R. Cheeseman, J. A. Montgomery, Jr., T. Vreven, K. N. Kudin, J. C. Burant, J. M. Millam, S. S. Iyengar, J. Tomasi, V. Barone, B. Mennucci, M. Cossi, G. Scalmani, N. Rega, G. A. Petersson, H. Nakatsuji, M. Hada, M. Ehara, K. Toyota, R. Fukuda, J. Hasegawa, M. Ishida, T. Nakajima, Y. Honda, O. Kitao, H. Nakai, M. Klene, X. Li, J. E. Knox, H. P. Hratchian, J. B. Cross, V. Bakken, C. Adamo, J. Jaramillo, R. Gomperts, R. E. Stratmann, O. Yazyev, A. J. Austin, R. Cammi, C. Pomelli, J. Ochterski, P. Y. Ayala, K. Morokuma, G. A. Voth, P. Salvador, J. J. Dannenberg, V. G. Zakrzewski, S. Dapprich, A. D. Daniels, M. C. Strain, O. Farkas, D. K. Malick, A. D. Rabuck, K. Raghavachari, J. B. Foresman, J. V. Ortiz, Q. Cui, A. G. Baboul, S. Clifford, J. Cioslowski, B. B. Stefanov, G. Liu, A. Liashenko, P. Piskorz, I. Komaromi, R. L. Martin, D. J. Fox, T. Keith, M. A. Al-Laham, C. Y. Peng, A. Nanayakkara, M. Challacombe, P. M. W. Gill, B. G. Johnson, W. Chen, M. W. Wong, C. Gonzalez and J. A. Pople, *GAUSSIAN 03 (Revision B.05)*, Gaussian, Inc., Wallingford, CT, 2004.

